

Robust design optimization for a nonlinear system via Bayesian neural network enhanced polynomial dimensional decomposition

Hyunho Jang^a, Dongjin Lee^{b,*}

^a Department of Automotive Engineering (Automotive-Computer Convergence), Hanyang University, Seoul, South Korea

^b Department of Automotive Engineering, Hanyang University, Seoul, South Korea

February 10, 2026

Abstract

Uncertainties such as manufacturing tolerances cause performance variations in complex engineering systems, making robust design optimization (RDO) essential. However, simulation-based RDO faces high computational cost for statistical moment estimation, and strong nonlinearity limits the accuracy of conventional surrogate models. This study proposes a novel RDO method that integrates Bayesian neural networks (BNN) with polynomial dimensional decomposition (PDD). The method employs uncertainty-based active learning to enhance BNN surrogate accuracy and a multi-point single-step strategy that partitions the design space into dynamically adjusted subregions, within which PDD analytically estimates statistical moments from BNN predictions. Validation through a mathematical benchmark and an electric motor shape optimization demonstrates that the method converges to robust optimal solutions with significantly fewer function evaluations. In the ten-dimensional benchmark, the proposed method achieved a 99.97% mean reduction, while Gaussian process-based and Monte Carlo approaches failed to locate the global optimum. In the motor design problem, the method reduced cogging torque by 94.75% with only 6644 finite element evaluations, confirming its computational efficiency for high-dimensional, strongly nonlinear engineering problems.

Keywords: Robust design optimization, Bayesian neural network, polynomial dimensional decomposition, surrogate model, uncertainty quantification

1. Introduction

Robust design optimization (RDO) derives designs insensitive to performance variations by minimizing the impact of uncertainty on system outputs. Since Taguchi's work [1], industries including aerospace, automotive, civil, and electronics have widely adopted RDO as a key technology to enhance product reliability [2, 3, 4, 5, 6]. In practice, engineering design processes face inherent uncertainties—such as manufacturing tolerances and material variations—that degrade the performance of nominal designs. These uncertainties are categorized into two primary types: epistemic uncertainty, which arises from model deficiencies in regions with insufficient training data and can be reduced by acquiring more data; and aleatoric uncertainty, which arises from inherent variability, such as manufacturing tolerances, and remains irreducible.

A commonly used RDO formulation includes objective and/or constraint functions using second-order statistical moments, such as the mean and variance of design and uncertain variables. This inherently relies on accurate estimation of these moments. Monte Carlo simulation (MCS) can estimate statistical moments but typically requires a large number of samples to achieve reliable convergence, resulting in high computational cost. To mitigate this, various surrogate models, including polynomial

*Corresponding author

Email address: dlee46@hanyang.ac.kr; +1 858-246-5327 (Dongjin Lee)

chaos expansion [7], Kriging [8], support vector machines [9], reduced order modeling [10], artificial neural networks [6], and more [11, 12, 13], have been used. However, these models often struggle to maintain predictive accuracy when encountering highly nonlinear responses with high-dimensional inputs. High-dimensional inputs make surrogate model construction computationally prohibitive due to the curse of dimensionality, where the required sample number increases exponentially. These models are generally classified into deterministic and probabilistic approaches. Deterministic surrogate models, such as standard artificial neural networks or polynomial chaos expansions, provide only point estimates and fail to account for epistemic uncertainty or prediction reliability. In contrast, probabilistic models quantify such prediction uncertainty. Gaussian process (GP) models—such as Kriging—offer inherent uncertainty quantification, but they become computationally inefficient for design problems with high-dimensional inputs because their training cost scales cubically with the sample number. Bayesian neural network (BNN) has emerged as a scalable alternative, addressing these computational bottlenecks while maintaining robust uncertainty quantification.

BNN offers a scalable probabilistic modeling approach for design problems with high-dimensional inputs and has been successfully applied across diverse engineering domains [14, 15, 16]. Unlike deterministic neural networks, BNN treats both network weights and biases as probability distributions rather than single-point estimates, thereby enabling explicit quantification of the model's epistemic uncertainty. This probabilistic formulation supports active learning strategies that prioritize sampling in high-variance regions, improving data efficiency and reliability at reduced computational cost. By leveraging a deep learning architecture, BNN captures complex variable interactions through hierarchical nonlinear mappings, mitigating the exponential parameter growth typical of high-dimensional problems. That said, maintaining accuracy across an expanding design space remains challenging, as the growing sample requirements still impose a significant computational burden.

To address the computational cost of iterative moment estimation in RDO, polynomial dimensional decomposition (PDD) surrogate offers an efficient alternative. PDD evaluates statistical moments via closed-form expressions derived from its expansion coefficients, scaling effectively by decomposing responses into low-order component functions [17]. However, this approach struggles with strongly nonlinear responses—such as cogging torque in electric motors—where polynomial bases fail to capture sharp local variations. Moreover, surrogates trained solely within the random variable space lack the extrapolation capability needed to maintain accuracy across the broader design space inherent to RDO [18]. A recent work on multi-point single-step (MPSS) RDO [19] addresses this limitation by partitioning the design space into subregions and solving localized RDO subproblems in a divide-and-conquer fashion. That said, MPSS RDO relies on gradient-based optimization, which becomes problematic for responses exhibiting severe nonlinearity—such as cogging torque in electric motors—where reliable gradient information is difficult to obtain, limiting its convergence and solution quality.

This paper proposes a novel RDO method that integrates BNN with PDD. The combined method leverages BNN as a surrogate to replace expensive model evaluations required for PDD coefficient calculation. This enables rapid estimation of statistical moments at significantly reduced computational cost. The proposed method maximizes sampling efficiency through an active learning strategy driven by BNN predictive uncertainty. The method adopts a MPSS method that partitions the design space into subregions and constructs local surrogate models, while using a global search within each subregion to handle severe nonlinearity. A dynamic resizing strategy further adjusts subregion boundaries during optimization to avoid entrapment in local optima and enhance search robustness. PDD is then applied to the resulting surrogate, exploiting the structural decomposition of component functions for efficient and accurate probabilistic analysis. The key contributions of this work are:

- (1) a novel integration of BNN and PDD that simultaneously achieves computational efficiency and prediction accuracy for nonlinear RDO problems with high-dimensional inputs;
- (2) an active learning sampling strategy that leverages predictive uncertainty to progressively enhance surrogate model reliability;
- (3) a dynamic subregion resizing strategy combined with global search that prevents local optima

and promotes robust convergence to the global solution.

The paper is organized as follows. Section 2 reviews the theoretical foundations underlying the proposed method. Section 3 formulates the RDO problems using transformed random variables to maximize computational efficiency of PDD basis functions. Section 3.3 details the step-by-step procedure of the overall optimization algorithm integrating the described components. Section 4 validates the proposed method through a mathematical benchmark and an electric motor design problem. Section 5 concludes the paper.

2. Theoretical background

This section presents the theoretical foundations of the proposed method. Section 2.1 defines the input and output random variables. Section 2.2 formulates the RDO problem. Section 2.3 summarizes PDD and details the calculation of statistical moments via its expansion coefficients. Section 2.4 describes BNN and its uncertainty quantification ability.

2.1. Input and output random variables

Consider a probability space $(\Omega, \mathcal{F}, \mathbb{P})$, where Ω denotes the sample space, \mathcal{F} represents a σ -algebra on Ω , and $\mathbb{P} : \mathcal{F} \rightarrow [0, 1]$ is a probability measure. We define an N -dimensional input random vector $\mathbf{X} := (X_1, \dots, X_N)^\top$ as a mapping from (Ω, \mathcal{F}) to a measurable space $(\mathbb{A}^N, \mathcal{B}^N)$. Here, $\mathbb{A}^N \subseteq \mathbb{R}^N$ denotes a subset of the real space, and \mathcal{B}^N denotes the Borel σ -algebra on \mathbb{A}^N .

We assume the input random variables to be mutually independent. We define the joint cumulative distribution function (CDF) of \mathbf{X} as $F_{\mathbf{X}}(\mathbf{x}) := \mathbb{P}[\cap_{i=1}^N \{X_i \leq x_i\}]$, and the corresponding joint probability density function (PDF) as $f_{\mathbf{X}}(\mathbf{x}) := \frac{\partial^N F_{\mathbf{X}}(\mathbf{x})}{\partial x_1 \dots \partial x_N}$. Under this independence assumptions, we factorize the joint PDF as $f_{\mathbf{X}}(\mathbf{x}) := \prod_{i=1}^N f_i(X_i)$, where $f_i(X_i)$ denotes the marginal PDF of the i -th random variable X_i . We then express the probability measure induced by \mathbf{X} as $(\mathbb{A}^N, \mathcal{B}^N, f_{\mathbf{X}}(\mathbf{x})d\mathbf{x})$.

Given the input random vector \mathbf{X} on $(\Omega, \mathcal{F}, \mathbb{P})$ and a model function $y : \mathbb{A}^N \rightarrow \mathbb{R}$, we define the output random variable as $Y = y(\mathbf{X}) : (\Omega, \mathcal{F}) \rightarrow (\mathbb{R}, \mathcal{B})$. We assume Y has a finite second moment, ensuring that both the mean and variance of Y are well-defined. The output Y captures the propagation of input uncertainty through the model $y(\cdot)$.

2.2. Robust design optimization

RDO seeks optimal designs by simultaneously accounting for the mean and variance of performance functions under aleatoric uncertainty. We define the design vector $\mathbf{d} = (d_1, \dots, d_M)^\top \in \mathcal{D} \subseteq \mathbb{R}^M$ as the mean values of a selected subset of input random variables \mathbf{X} , where $M \leq N$. Here, \mathbf{X} represents aleatoric uncertainty arising from inherent variability in the system. This definition reflects the fact that the mean corresponds to the nominal value—a controllable quantity in actual manufacturing. We generally treat the standard deviations as fixed parameters determined by manufacturing capability. However, in specific situations such as tolerance design, we can treat standard deviations as additional design variables.

The PDF of the input random variables \mathbf{X} depends on the design vector \mathbf{d} , which we express as $f_{\mathbf{X}}(\mathbf{x}; \mathbf{d})$. We formulate the general RDO problem as

$$\begin{aligned} \min_{\mathbf{d} \in \mathcal{D} \subseteq \mathbb{R}^M} \quad & c_0(\mathbf{d}) := g_0(\mathbb{E}_{\mathbf{d}}[y_0(\mathbf{X})], \text{Var}_{\mathbf{d}}[y_0(\mathbf{X})]), \\ \text{subject to} \quad & c_l(\mathbf{d}) := g_l(\mathbb{E}_{\mathbf{d}}[y_l(\mathbf{X})], \text{Var}_{\mathbf{d}}[y_l(\mathbf{X})]) \leq 0, \\ & l = 1, \dots, K, \\ & d_{k,L} \leq d_k \leq d_{k,U}, \quad k = 1, \dots, M, \end{aligned}$$

where $\mathbb{E}_{\mathbf{d}}[y_l(\mathbf{X})] := \int_{\mathbb{R}^N} y_l(\mathbf{x}) f_{\mathbf{X}}(\mathbf{x}; \mathbf{d}) d\mathbf{x}$ denotes the mean of $y_l(\mathbf{X})$, and $\text{Var}_{\mathbf{d}}[y_l(\mathbf{X})] := \mathbb{E}_{\mathbf{d}}[(y_l(\mathbf{X}) - \mathbb{E}_{\mathbf{d}}[y_l(\mathbf{X})])^2]$ represents the variance of $y_l(\mathbf{X})$. The functions $g_0(\cdot)$ and $g_l(\cdot)$ represent arbitrary compositions of the mean and variance, and $d_{k,L}$ and $d_{k,U}$ denote the lower and upper bounds of each design variable d_k , respectively.

In practice, we specify this general RDO formulation into concrete mathematical forms. We adopt the weighted sum method, a widely approach, formulated as

$$\min_{\mathbf{d} \in \mathcal{D} \subseteq \mathbb{R}^M} c_0(\mathbf{d}) := w_1 \frac{\mathbb{E}_{\mathbf{d}}[y_0(\mathbf{X})]}{\mu_0} + w_2 \frac{\sqrt{\text{Var}_{\mathbf{d}}[y_0(\mathbf{X})]}}{\sigma_0}, \quad (1)$$

where $w_1, w_2 \geq 0$ are weights satisfying $w_1 + w_2 = 1$, and μ_0 and σ_0 are non-zero, real-valued scaling factors. We typically express the constraints as

$$c_l(\mathbf{d}) := \alpha_l \sqrt{\text{Var}_{\mathbf{d}}[y_l(\mathbf{X})]} - \mathbb{E}_{\mathbf{d}}[y_l(\mathbf{X})] \leq 0, \quad l = 1, \dots, K, \quad (2)$$

where α_l are non-negative, real-valued constants associated with the probabilities of constraint satisfaction. Each constraint enforces robustness by guaranteeing that the system performance remains within the feasible region despite inherent variability.

2.3. Polynomial dimensional decomposition

PDD uses the analysis-of-variance (ANOVA) decomposition to analyze statistical moments of multivariate functions. The ANOVA decomposition expresses a multivariate function as a sum of component functions of increasing interaction order—comprising a constant term, univariate effects, and multivariate interactions among input variable subsets. PDD can represents any square-integrable function on the probability space $(\Omega, \mathcal{F}, \mathbb{P})$ through an infinite Fourier-like polynomial expansion [17]. For computational efficiency, we adopt the S -variate, m -th order PDD approximation. This truncates the expansion by retaining only interaction orders up to S and polynomial orders up to m . We define the truncated PDD approximation $\tilde{y}_{S,m}(\mathbf{X})$ as

$$\tilde{y}_{S,m}(\mathbf{X}) := y_0 + \sum_{\substack{\emptyset \neq u \subseteq \{1, \dots, N\} \\ 1 \leq |u| \leq S}} \sum_{\substack{\mathbf{j}_{|u|} \in \mathbb{N}^{|u|} \\ |u| \leq |\mathbf{j}_{|u|}| \leq m}} c_{u\mathbf{j}_{|u|}} \psi_{u\mathbf{j}_{|u|}}(\mathbf{X}_u) \approx y(\mathbf{X}), \quad (3)$$

where $y_0 = \int_{\mathbb{A}^N} y(\mathbf{X}) f_{\mathbf{X}}(\mathbf{x}) d\mathbf{x}$ denotes the mean of the function. In (3), $u \subseteq \{1, \dots, N\}$ denotes a non-empty subset of the variable indices with cardinality $|u|$, and $\mathbf{j}_{|u|} = (j_{i_1}, \dots, j_{i_{|u|}}) \in \mathbb{N}^{|u|}$ is a multi index whose component j_{i_k} specifies the polynomial order for variable X_{i_k} . We define the expansion coefficient $c_{u\mathbf{j}_{|u|}}$ and the multivariate basis function $\psi_{u\mathbf{j}_{|u|}}(\mathbf{X}_u)$ as

$$\begin{aligned} c_{u\mathbf{j}_{|u|}} &:= \int_{\mathbb{A}^N} y(\mathbf{x}) \psi_{u\mathbf{j}_{|u|}}(\mathbf{x}_u) f_{\mathbf{X}}(\mathbf{x}) d\mathbf{x}, \\ \psi_{u\mathbf{j}_{|u|}}(\mathbf{X}_u) &= \prod_{i \in u} \psi_{i,j_i}(\mathbf{X}_i). \end{aligned}$$

Here, ψ_{i,j_i} is a univariate polynomial of order j_i that satisfies orthonormality with respect to the marginal probability density function $f_{X_i}(x_i) dx_i$ of variable X_i . These basis functions satisfy the following orthonormality condition:

$$\begin{aligned} \mathbb{E}[\psi_{u\mathbf{j}_{|u|}}(\mathbf{X}_u)] &= \begin{cases} 1, & \mathbf{j}_{|u|} = \mathbf{0}, \\ 0, & \text{otherwise.} \end{cases} \\ \mathbb{E}[\psi_{u\mathbf{j}_{|u|}}(\mathbf{X}_u) \psi_{v\mathbf{k}_{|v|}}(\mathbf{X}_v)] &= \begin{cases} 1, & u = v \text{ and } \mathbf{j}_{|u|} = \mathbf{k}_{|v|}, \\ 0, & \text{otherwise,} \end{cases} \end{aligned}$$

where $v \subseteq \{1, \dots, N\}$ is another non-empty set of variable indices and $\mathbf{k}_{|v|} \in \mathbb{N}^{|v|}$ is the corresponding multi-index, analogous to u and $\mathbf{j}_{|u|}$.

For notational convenience, we re-index the multi-index basis functions into a single index $\{\psi_i(\mathbf{X})\}_{i=1}^{L_{N,S,m}}$. The total number of basis functions $L_{N,S,m} = 1 + \sum_{s=1}^S \binom{N}{s} \binom{m}{s}$ depends on the truncation parameters S and m . We then express the truncated PDD as a linear combination:

$$\tilde{y}_{S,m}(\mathbf{X}) = \sum_{i=1}^{L_{N,S,m}} c_i \Psi_i(\mathbf{X}),$$

with the expansion coefficient vector $\mathbf{c} = (c_1, \dots, c_{L_{N,S,m}})^\top \in \mathbb{R}^{L_{N,S,m}}$. We estimate \mathbf{c} via least squares by evaluating the function at \bar{L} sample points, yielding the linear system:

$$\underbrace{\begin{bmatrix} \psi_1(\mathbf{x}^{(1)}) & \dots & \psi_{L_{N,S,m}}(\mathbf{x}^{(1)}) \\ \vdots & \ddots & \vdots \\ \psi_1(\mathbf{x}^{(\bar{L})}) & \dots & \psi_{L_{N,S,m}}(\mathbf{x}^{(\bar{L})}) \end{bmatrix}}_{=: \mathbf{A} \in \mathbb{R}^{\bar{L} \times L_{N,S,m}}} \underbrace{\begin{bmatrix} c_1 \\ \vdots \\ c_{L_{N,S,m}} \end{bmatrix}}_{=: \mathbf{c} \in \mathbb{R}^{L_{N,S,m}}} = \underbrace{\begin{bmatrix} y(\mathbf{x}^{(1)}) \\ \vdots \\ y(\mathbf{x}^{(\bar{L})}) \end{bmatrix}}_{=: \mathbf{b} \in \mathbb{R}^{\bar{L}}},$$

from which we obtain

$$\mathbf{c} = (\mathbf{A}^\top \mathbf{A})^{-1} \mathbf{A}^\top \mathbf{b}.$$

Exploiting the orthonormality of the basis functions, we analytically derive the mean and variance [20] of $\tilde{y}_{S,m}(\mathbf{X})$ directly from the expansion coefficients:

$$\mathbb{E}[\tilde{y}_{S,m}(\mathbf{X})] = c_1, \quad \text{Var}[\tilde{y}_{S,m}(\mathbf{X})] = \sum_{i=2}^{L_{N,S,m}} c_i^2. \quad (4)$$

2.4. Bayesian neural networks

Artificial neural networks model complex nonlinear relationship between an input vector \mathbf{x} and output $y(\mathbf{x})$ through multi-layer neuron structures, i.e., $y(\mathbf{x}) \simeq \tilde{y}_{\mathcal{N}}(\mathbf{x}; \boldsymbol{\theta})$. Here, $\boldsymbol{\theta} = (\omega_1, \dots, \omega_{L_\omega}, b_1, \dots, b_{L_b})^\top$ denotes the model parameters. Also, ω_i for $i = 1, \dots, L_\omega$ are the weights and b_j for $j = 1, \dots, L_b$ are the biases, both determined through training. A conventional deterministic neural network identifies a single optimal parameter set that minimizes a loss function, such as the mean squared error between predicted and observed values. This point estimation approach fails to capture the epistemic uncertainty inherent in the model itself. In contrast, BNN quantifies epistemic uncertainty by assigning probability distributions to the model parameters rather than treating them as deterministic values [21].

BNN, similar to GP, relies on Bayesian inference by treating the model parameters as a random vector $\boldsymbol{\Theta}$, which maps from (Ω, \mathcal{F}) to a measurable space $(\mathbb{A}^{L_\omega+L_b}, \mathcal{B}^{L_\omega+L_b})$, with realizations $\boldsymbol{\theta} \in \mathbb{R}^{L_\omega+L_b}$. GP requires computational cost proportional to the cube of the data size due to covariance matrix inversion, making it impractical for large datasets. BNN, however, scales more efficiently through mini-batch stochastic optimization, where the training cost per iteration grows only linearly with data size. Moreover, while GP suffers from degraded kernel function performance in high-dimensional inputs, BNN effectively captures complex variable interactions through the hierarchical structure of neural networks.

Following standard convention in Bayesian modeling, we use $p(\cdot)$ to denote prior, posterior, and likelihood distributions throughout this section. Given a training dataset $\mathcal{S} = \{\mathbf{x}^{(l)}, y(\mathbf{x}^{(l)})\}_{l=1}^L$, we define the posterior distribution of the model parameters via Bayes' theorem, i.e.,

$$p(\boldsymbol{\theta}|\mathcal{S}) = \frac{p(\mathcal{S}|\boldsymbol{\theta})p(\boldsymbol{\theta})}{p(\mathcal{S})},$$

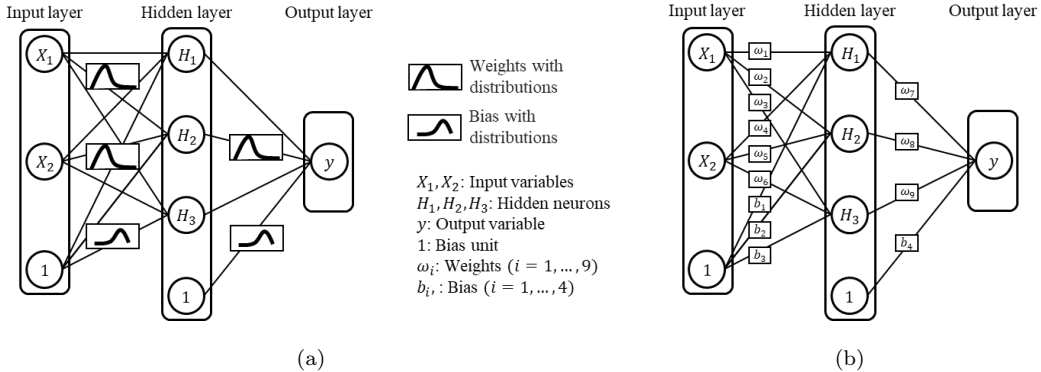


Figure 1: Schematic diagram of the neural network architecture. The network consists of input nodes (X_1, X_2) and a bias unit denoted by 1, which provides a constant input value. Also, ω denotes the weights, and b represents the biases. Each hidden neuron (H_1, H_2, H_3) applies a nonlinear activation function to the weighted sum of its inputs: (a) Bayesian neural networks; (b) Artificial neural network

where $p(\theta)$ is the prior distribution over the parameters and $p(S|\theta)$ is the likelihood. The prior constrains the model parameters during training, effectively preventing overfitting without requiring a separate regularization term [22]. The denominator, $p(S) = \int p(S|\theta)p(\theta)d\theta$, is called the evidence or marginal likelihood, function as a normalization constant indicating how well the model explains the data. However, in the context of deep neural networks, the high dimensionality of the weights makes the analytical calculation of the evidence through integration intractable. To address this challenge, variational inference serves as a standard approach [23, 24].

Variational inference approximates the true posterior $p(\theta|S)$ with a tractable distribution $q(\theta|\phi)$ parameterized by the variational parameters ϕ . The objective is to minimize the Kullback-Leibler (KL) divergence between the approximate and true posterior distributions, i.e., $D_{KL}(q(\theta|\phi)||p(\theta)) = \sum_{\theta} p(\theta) \log \frac{p(\theta)}{q(\theta|\phi)}$. Since directly minimizing this KL divergence requires the intractable true posterior, we equivalently maximize the evidence lower bound (ELBO) as

$$\mathcal{L}_{\text{ELBO}} = \mathbb{E}_{q(\boldsymbol{\theta}|\boldsymbol{\phi})}[\log p(\mathcal{S}|\boldsymbol{\theta})] - D_{KL}(q(\boldsymbol{\theta}|\boldsymbol{\phi})||p(\boldsymbol{\theta})).$$

The first term measures the model's goodness of fit to the given data, and the second KL divergence term regularizes the approximate posterior to remain close to the prior. Maximizing the ELBO updates the variational parameters θ , driving the approximate posterior $q(\theta|\phi)$ toward the true posterior.

We obtain the predictive distribution for the output $\tilde{y}_N^* = \tilde{y}_N(\mathbf{x}^*; \boldsymbol{\theta})$ at a new test input \mathbf{x}^* by marginalizing over the posterior as

$$p(\tilde{y}_N^* | \mathbf{x}^*, \mathcal{S}) = \int p(\tilde{y}_N^* | \mathbf{x}^*, \boldsymbol{\theta}) \cdot p(\boldsymbol{\theta} | \mathcal{S}) d\boldsymbol{\theta}.$$

The nonlinear activation functions and multi-layer structure of neural networks prevent a closed-form solution for this integral. We thus use Monte Carlo approximation by drawing T weight samples $\boldsymbol{\theta}^{(t)}$ from the approximate posterior $q(\boldsymbol{\theta}|\boldsymbol{\phi})$ as

$$p(\tilde{y}_{\mathcal{N}}^* | \mathbf{x}^*, \mathcal{S}) \approx \frac{1}{T} \sum_{t=1}^T p(\tilde{y}_{\mathcal{N}}^* | \mathbf{x}^*, \boldsymbol{\theta}^{(t)}).$$

We then derive the predictive mean and variance as

$$\mathbb{E}[\tilde{y}_{\mathcal{N}}(\mathbf{x}^*; \boldsymbol{\Theta})|\mathcal{S}] = \tilde{\mu}_{\tilde{y}_{\mathcal{N}}}(\mathbf{x}^*; \boldsymbol{\Theta}) \approx \frac{1}{T} \sum_{t=1}^T \tilde{y}_{\mathcal{N}}(\mathbf{x}^*; \boldsymbol{\theta}^{(t)}), \quad (5)$$

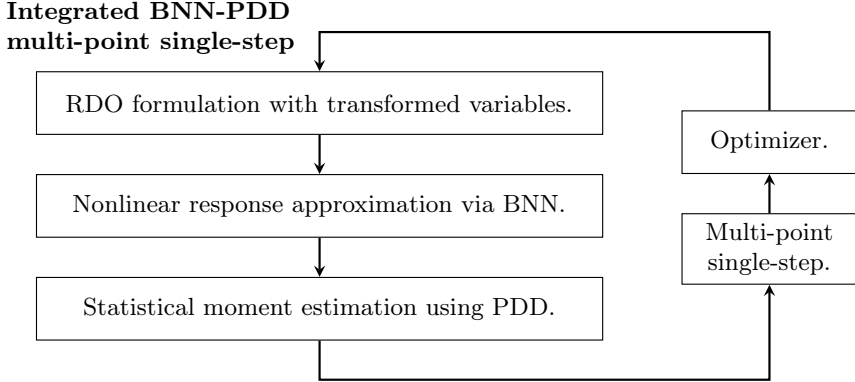
$$\text{Var}[\tilde{y}_{\mathcal{N}}(\mathbf{x}^*; \boldsymbol{\Theta})|\mathcal{S}] = \tilde{\sigma}_{\tilde{y}_{\mathcal{N}}}^2(\mathbf{x}^*; \boldsymbol{\Theta}) \approx \frac{1}{T} \sum_{t=1}^T \tilde{y}_{\mathcal{N}}(\mathbf{x}^*; \boldsymbol{\theta}^{(t)})^2 - \left(\frac{1}{T} \sum_{t=1}^T \tilde{y}_{\mathcal{N}}(\mathbf{x}^*; \boldsymbol{\theta}^{(t)}) \right)^2, \quad (6)$$

where $\tilde{y}_{\mathcal{N}}(\mathbf{x}^*; \boldsymbol{\theta}^{(t)})$ represents the neural networks output using the t -th weight sample. The predictive mean $\tilde{\mu}_{\tilde{y}_{\mathcal{N}}}$ represents the ensemble-average output, and the predictive variance $\tilde{\sigma}_{\tilde{y}_{\mathcal{N}}}$ quantifies the epistemic uncertainty, reflecting the model's confidence in its prediction.

3. Robust design optimization with BNN-PDD integration

This section proposes a novel method that combines efficient surrogate modeling with UQ to address the computational challenges of RDO. The proposed method leverages the predictive uncertainty from Bayesian inference to enable efficient exploration of the design space. Section 3.1 formulates the RDO problem using transformed random variables. Section 3.2 details the BNN-based single-step process, which integrates active learning for surrogate construction with the BNN-PDD method for statistical moment estimation. Section 3.3 extends this method to a multi-point single-step process. Section 3.4 outlines the complete algorithm of the proposed RDO framework. Figure 2 illustrates the overall procedure, comprising variable transformation, nonlinear response approximation via BNN, and moment estimation through PDD.

Figure 2: The overall framework of the proposed BNN-PDD multi-point single-step optimization.



3.1. Robust design optimization with transformed random variables

The RDO estimates the mean and variance of system performance under uncertainty and derives an optimal design based on these statistics. During the optimization process, the probability distribution of \mathbf{X} changes whenever design variables are updated. Since PDD basis functions must satisfy orthogonality with respect to the input PDF, this variation requires recalculating the basis functions at every iteration, resulting in substantial computational cost.

To overcome this computational burden, we introduce transformed variables $\mathbf{U} = (U_1, \dots, U_N)^\top$ that follow a fixed probability distribution independent of the design variables. Without loss of generality, we adopt the uniform distribution as a representative example. We assume each component of \mathbf{U} follows a uniform distribution on a fixed interval $[\mathbf{a}, \mathbf{b}] \subset \mathbb{R}^N$, where $\mathbf{a} = (a_1, \dots, a_N)^\top$ and $\mathbf{b} = (b_1, \dots, b_N)^\top$ denote the lower and upper bound vectors, respectively. This formulation allows us to compute the PDD basis functions only once for the fixed uniform distribution, eliminating recalculation throughout the design iterations and significantly enhancing computational efficiency.

We map the transformed variables \mathbf{U} to the original random variables \mathbf{X} via the probability integral transformation. The joint CDF of \mathbf{U} on $[\mathbf{a}, \mathbf{b}]$ is

$$F_{\mathbf{U}}(\mathbf{u}) = \prod_{i=1}^N \frac{u_i - a_i}{b_i - a_i}, \quad \mathbf{u} \in [\mathbf{a}, \mathbf{b}].$$

We denote the CDF of \mathbf{X} as $F_{\mathbf{X}}(\mathbf{x}; \mathbf{d})$ as the CDF depends on the design vector \mathbf{d} . Equating $F_{\mathbf{X}}(\mathbf{x}; \mathbf{d})$, we obtain the inverse mapping, i.e.,

$$\mathbf{x} = F_{\mathbf{X}}^{-1} \left(\frac{\mathbf{u} - \mathbf{a}}{\mathbf{b} - \mathbf{a}}; \mathbf{d} \right), \quad (7)$$

where $F_{\mathbf{X}}^{-1}(\cdot)$ denotes the inverse CDF of \mathbf{X} . We note that the optimization still proceeds in the design variable space; the transformation only changes the domain over which we compute the statistical moments—from the design dependent \mathbf{X} to the fixed \mathbf{U} distribution. We formulate the RDO problem using the transformed functions $y_l(\mathbf{X}) = y_l(F_{\mathbf{X}}^{-1}(\Phi(\mathbf{U}); \mathbf{d})) = h_l(\mathbf{U}; \mathbf{d})$, $l = 0, 1, \dots, K$, as

$$\begin{aligned} \min_{\mathbf{d} \in \mathcal{D} \subseteq \mathbb{R}^M} \quad & c_0(\mathbf{d}) := w_1 \frac{\mathbb{E}[h_0(\mathbf{U}; \mathbf{d})]}{\mu_0} + w_2 \frac{\sqrt{\text{Var}[h_0(\mathbf{U}; \mathbf{d})]}}{\sigma_0}, \\ \text{subject to} \quad & c_l(\mathbf{d}) := \alpha_l \sqrt{\text{Var}[h_l(\mathbf{U}; \mathbf{d})]} - \mathbb{E}[h_l(\mathbf{U}; \mathbf{d})] \leq 0, \quad l = 1, \dots, K, \\ & d_{k,L} \leq d_k \leq d_{k,U}, \quad k = 1, \dots, M. \end{aligned} \quad (8)$$

This formulation enables the reuse of PDD basis function across all design iterations, significantly reducing computational cost while maintaining accuracy in statistical moment estimation.

3.2. BNN based single step process

This section presents an integrated framework for efficient statistical moment calculation in RDO. We first construct a BNN surrogate to approximate the system response, and then combine it with the transformed variable formulation and PDD for moment estimation.

3.2.1. BNN modeling via active learning

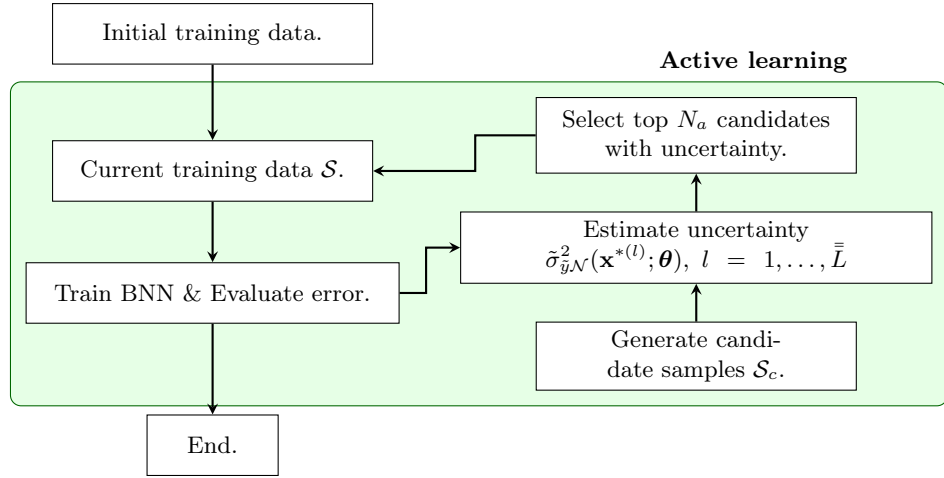


Figure 3: Flowchart of the active learning algorithm using BNN.

We construct a BNN surrogate model within the physical design space to approximate the input-output relationship of the system. To acquire training data efficiently, we use Latin hypercube sampling (LHS) [25, 26], which explores the design domain uniformly regardless of the probability distributions of design variables or transformed variables. We generate training samples via LHS and

evaluate the corresponding response values from the original model to construct the initial dataset \mathcal{S} . The predictive performance of BNN (see Section 2.4) depends on hyperparameter settings. Instead of using fixed hyperparameters, we apply GP-based Bayesian optimization to determine the optimal hyperparameters for the dataset \mathcal{S} . With these optimal hyperparameters, BNN learns the posterior distribution of the weights and provides both predictive values and uncertainty estimates for arbitrary inputs.

RDO requires maximizing surrogate model accuracy within a limited computational budget. Conventional random sampling, however, neglects model uncertainty, potentially leading to inefficient sampling placement. To address this, we use an uncertainty-based active learning strategy that leverages the epistemic uncertainty from BNN to reinforce regions of low model confidence.

Fig. 3 illustrates that the active learning algorithm operates through the following iterative procedure. We first generate \bar{L} candidate samples $\mathcal{S}_c = \{\mathbf{x}^{*(l)}\}_{l=1}^{\bar{L}}$ through LHS within the currently defined subregion. We then evaluate the prediction variance $\tilde{\sigma}_{\mathcal{Y}N}^2(\mathbf{x}^{*(l)}; \boldsymbol{\theta})$ for each candidate $\mathbf{x}^{*(l)}$ using the trained BNN via (6). We sort all candidates in descending order of their predictive variance and select the top N_a samples with the highest uncertainty, i.e.,

$$\mathcal{S}_a = \left\{ \mathbf{x}^{*(l)} \in \mathcal{S}_c \mid \tilde{\sigma}_{\mathcal{Y}N}^2(\mathbf{x}^{*(l)}; \boldsymbol{\theta}) \geq \tilde{\sigma}_{\mathcal{Y}N}^2(\mathbf{x}^{*(N_a)}; \boldsymbol{\theta}), l = 1, \dots, \bar{L} > N_a \right\}.$$

Since these samples reside in regions where the model lacks confidence, we evaluate the original model at the selected samples to obtain actual response values and augment the training dataset accordingly. We then retain the BNN on the updated dataset, improving prediction accuracy in previously uncertain regions. We access convergence by computing the relative error between the retrained model's predictions and the actual values for the newly added N_a samples. We repeat this process until either the relative error falls below an acceptable threshold or the total number of training samples reaches a preset maximum. This active learning strategy enhances both computational efficiency and surrogate efficiency by concentrating function evaluations in regions of high uncertainty while avoiding unnecessary sampling elsewhere.

3.2.2. Statistical moment analysis via BNN-PDD

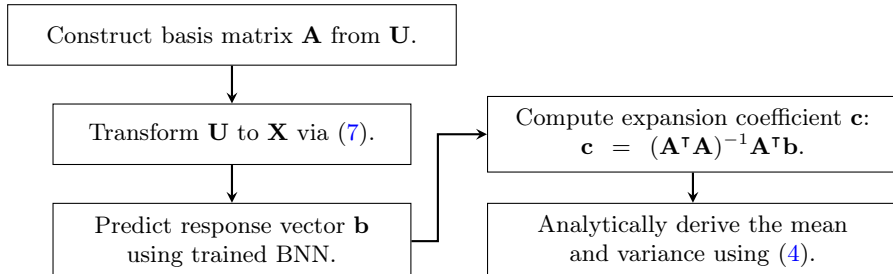


Figure 4: Flowchart of the statistical moment analysis using the proposed BNN-PDD method.

We combine BNN for approximating nonlinear system responses with PDD for estimating statistical moments. When using BNN alone, statistical moment estimation relies on MCS, which suffers from slow convergence and numerical instability due to stochastic sampling noise. In contrast, PDD derives the mean and variance from expansion coefficients in closed-form expression, yielding noise-free, deterministic values throughout the optimization process. The proposed integration thus leverages the nonlinear approximation ability of BNN and the analytical efficiency of PDD, offering better numerical stability and computational performance compared to MCS.

We apply the transformed variable formulation from Section 3.1 to eliminate the cost of recomputing orthonormal polynomials whenever design variables change. To maximize the estimation accuracy of PDD expansion coefficients, we use the Sobol sequence—a low-discrepancy sequence that distributes

samples uniformly even in high-dimensional spaces. This quasi-random sampling satisfies the orthogonality of PDD basis functions with fewer samples and accelerates convergence compared to simple random sampling.

Figure 4 illustrates the overall computational procedure. We first precompute and fix the basis matrix \mathbf{A} using Legendre polynomials evaluated at the Sobol-generated \mathbf{U} samples; this calculation occurs only once before optimization begins. At each optimization iteration, given a design vector \mathbf{d} , we convert \mathbf{U} to \mathbf{X} through the inverse transformation in (7) and feed the resulting \mathbf{X} into the trained BNN to predict the response vector \mathbf{b} . We then compute the expansion coefficient vector as $\mathbf{c} = (\mathbf{A}^\top \mathbf{A})^{-1} \mathbf{A}^\top \mathbf{b}$ via least squares. Exploiting the orthonormality of the basis functions, we analytically obtain the mean and variance from \mathbf{c} using (4) without additional simulations, and directly evaluate the RDO objective and constraint functions in (1). This procedure reduces statistical moment estimation to a sequence of variable transformation and matrix operations, completely avoiding basis function reconstruction across design iterations.

3.3. Multi-point single-step process via BDD-PDD

The single-step method in Section 3.2 constructs a BNN surrogate over the entire design space \mathcal{D} . For large design spaces or highly nonlinear responses, however, this global approach demands high-order basis functions or numerous samples for accurate approximation, degrading computational efficiency. A lower-accuracy approximation resulting from limited training samples may also fail to locate the true global optimum.

To address these challenges, we adopt a multi-point single-step (MPSS) strategy that decomposes the original RDO problem into a series of local RDO subproblems, where the objective and constraint functions in each subproblem are approximated within the corresponding local region [27].

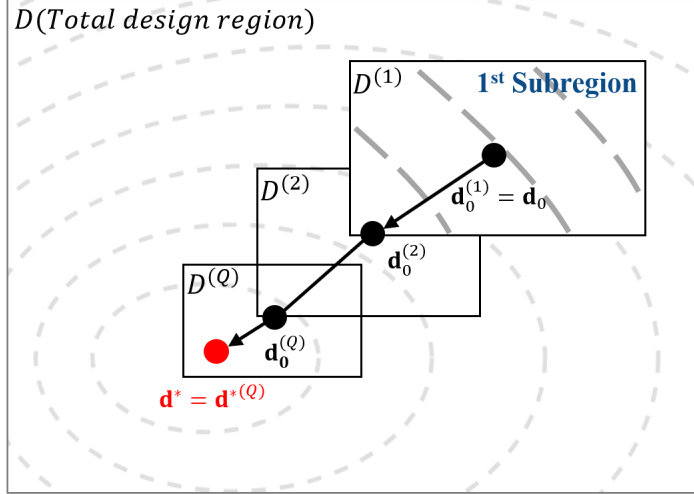


Figure 5: Schematic description of the multi-point single-step process.

Figure 5 illustrates the MPSS process. At the q -th iteration, we define a subregion $\mathcal{D}^{(q)}$ centered on the current initial design point $\mathbf{d}_0^{(q)}$ within the global design space $\mathcal{D} = \prod_{k=1}^M [d_{k,L}, d_{k,U}]$ as

$$\mathcal{D}^{(q)} = \prod_{k=1}^M \left[d_{k,0}^{(q)} - \beta_k^{(q)} \frac{(d_{k,U} - d_{k,L})}{2}, d_{k,0}^{(q)} + \beta_k^{(q)} \frac{(d_{k,U} - d_{k,L})}{2} \right], \quad q = 1, \dots, Q.$$

Here, $0 < \beta_k^{(q)} \leq 1$ is the sizing parameter controlling the subregion extent for the k -th design variable. We solve each subproblem using low-order BNN-PDD approximations within the defined subregion. The optimal design solution derived from the current subproblem then serves as the initial design point for the next iteration. We update $\beta_k^{(q)}$ and repeat this process until convergence to the optimum.

3.4. The complete algorithm for robust design optimization

Figure 6: Flowchart of the multi-point single-step BNN-PDD RDO algorithm.

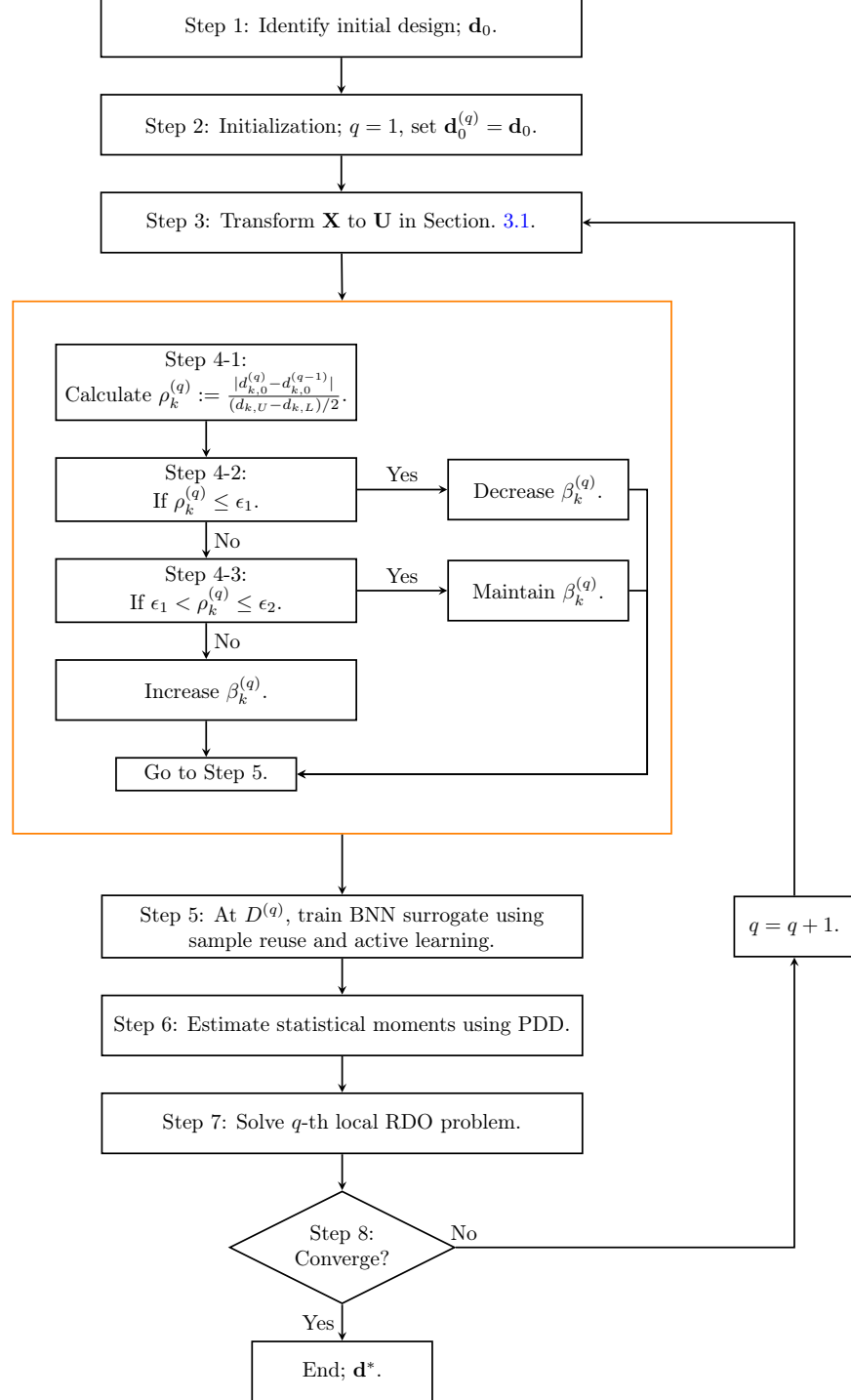


Figure 6 illustrates the complete procedure of the proposed RDO algorithm. We detail each step below.

Step 1: We determine an initial design vector \mathbf{d}_0 by first generating training data through LHS over

the entire design space \mathcal{D} and constructing an initial BNN model that captures the global trend. We apply the active learning strategy from Section 3.2.1 to ensure the reliability of this initial model. We then perform an approximate global optimization using (8) and set the resulting solution as the starting point \mathbf{d}_0 . Go to Step 2.

- Step 2: We set the subregion iteration index $q = 1$ and designate $\mathbf{d}_0^{(q)} = \mathbf{d}_0$ as the center of the first subregion. We also initialize the subregion parameters required for algorithm execution, including the subregion sizing parameter $\beta_k^{(q)}$ and convergence tolerances. Go to Step 3.
- Step 3: We apply the variable transformation in (7), mapping the input random variable \mathbf{X} to the transformed variable \mathbf{U} that follows a fixed uniform distribution. Go to Step 4.
- Step 4: We compute the normalized displacement

$$\rho_k^{(q)} := \frac{|d_{k,0}^{(q)} - d_{k,0}^{(q-1)}|}{(d_{k,U} - d_{k,L})/2},$$

defined as the ratio of the center point movement to half the global design range. We then update the sizing parameter $\beta_k^{(q)}$ according to the following rule:

if $\rho_k^{(q)} \leq \epsilon_1$: decrease $\beta_k^{(q)}$ (solution approaching convergence; contract the subregion);
 if $\epsilon_1 < \rho_k^{(q)} \leq \epsilon_2$: maintain $\beta_k^{(q)}$ (search range adequate);
 otherwise: increase $\beta_k^{(q)}$ (solution still exploring; expand the subregion).

This adaptive sizing enables the algorithm to begin with a broad search region and progressively narrow it as the solution converges toward the optimum. Go to Step 5.

- Step 5: We train the BNN surrogate within the current subregion $\mathcal{D}^{(q)}$ using two strategies for data efficiency. First, we identify the overlap between the current subregion $\mathcal{D}^{(q)}$ and the previous one $\mathcal{D}^{(q-1)}$, and directly reuse existing training samples within this region without additional model evaluations. Second, we apply the uncertainty-based active learning from Section 3.2.1 to add new samples in regions of high predictive uncertainty, improving surrogate prediction accuracy where it is most needed. Go to Step 6.
- Step 6: We analytically compute the mean and variance of the response function via (4) using the trained BNN model and the precomputed PDD basis functions. Go to Step 7.
- Step 7: We solve the local RDO problem within $\mathcal{D}^{(q)}$ using the estimated statistical moments, obtaining the optimal solution $\mathbf{d}^{*(q)}$. Go to Step 8.
- Step 8: We evaluate convergence by checking the following criteria between the current optimal design $\mathbf{d}^{*(q)}$ and the current initial design $\mathbf{d}_0^{(q)}$: if $\|\mathbf{d}^{*(q)} - \mathbf{d}_0^{(q)}\| \leq \epsilon_3$ or $\|c_0(\mathbf{d}^{*(q)}) - c_0(\mathbf{d}_0^{(q)})\| \leq \epsilon_4$, the algorithm terminates and outputs $\mathbf{d}^* = \mathbf{d}^{*(q)}$ as the final optimum. Otherwise, we set $\mathbf{d}_0^{(q+1)} = \mathbf{d}^{*(q)}$, increment $q = q + 1$, and return to Step 3.

4. Numerical examples

This section presents two numerical examples to validate the effectiveness and computational efficiency of the proposed BNN-PDD multi-point single-step RDO framework. Section 4.1 uses a benchmark mathematical RDO problem to evaluate the global search ability and convergence stability of the proposed algorithm. Section 4.2 demonstrates applicability to high-dimensional problems through a shape RDO for an electric motor.

In Example 1, we compare the proposed method against Gaussian process (GP) regression using the same number of training samples for objective performance evaluation. GP is a nonparametric Bayesian model that assumes function values follow a multivariate normal distribution, defining a zero-mean prior $y(\mathbf{x}) \sim \mathcal{GP}(0, k(\mathbf{x}, \mathbf{x}'))$ for the latent function $y(\mathbf{x})$, where $k(\mathbf{x}, \mathbf{x}')$ denotes the covariance function. We use the Matérn kernel $k(\mathbf{x}, \mathbf{x}') = \sigma^2 \frac{2^{1-\nu}}{\Gamma(\nu)} (\sqrt{2\nu} \frac{r}{\ell})^\nu K_\nu(\sqrt{2\nu} \frac{r}{\ell})$ to control function smoothness. Here, $\sigma^2 > 0$ is the signal variance controlling the overall amplitude of the function, $r = \|\mathbf{x} - \mathbf{x}'\|$ is the Euclidean distance between two points, $\Gamma(\cdot)$ is the gamma function, $K_\nu(\cdot)$ is the modified Bessel function of the second kind, $\ell > 0$ is the length scale controlling the rate of variation, and $\nu > 0$ is the smoothness parameter determining the differentiability order of the function.

In both examples, we formulate the problem as multi-objective optimization that simultaneously minimizes the mean and variance of the responses, and apply the weighted sum method to convert the multi-objective into a single objective function. For all cases, we set the PDD truncation parameters as polynomial order $m = 3$ and interaction order $S = 1$. Convergence tests confirmed that moment estimates exhibit negligible changes beyond these orders. We define the tolerance and subregion control parameters for MPSS algorithm as $\epsilon_1 = 0.1$, $\epsilon_2 = 0.5$, and $\epsilon_3 = \epsilon_4 = 0.01$, with an initial subregion sizing parameter of $\beta_k^{(1)} = 0.15$. For the local optimizer at each step, we adopt the differential evolution (DE) algorithm, which provides effective gradient-free global search for multi-modal objective functions. Comparative test with genetic algorithm (GA) showed that DE achieves faster convergence and better solutions quality. We obtain all numerical results using Python 3.11 on an Intel i5-13400 processor with 32 GB of RAM. The finite element analysis (FEA) in Example 2 was performed using JMAG (version 23.2).

4.1. Example 1: RDO of a benchmark mathematical function

We validate the performance of the proposed RDO algorithm through a mathematical benchmark. We compare three approaches: (1) the proposed BNN-PDD MPSS method, (2) GP-PDD MPSS which replaces BNN with GP as the surrogate model under the same domain settings and active learning strategy, and (3) MCS, which directly performs MCS over the global design space without a surrogate model. We consider two cases: a low-dimensional setting (Case 1: $N = 2$) and a high-dimensional setting (Case 2: $N = 10$).

4.1.1. Problem definition

We model each random variable X_i as a truncated Gaussian distribution with mean d_i and standard deviation σ_i . We determine σ_i applying the 3σ rule to a manufacturing tolerance of ± 0.01 , yielding $\sigma_i = 0.01/3$. We formulate the RDO problem to minimize the weighted sum of the mean and standard deviation as defined in (1):

$$\begin{aligned} \min_{\mathbf{d} \in \mathcal{D}} \quad c_0(\mathbf{d}) = & w_1 \frac{\mathbb{E}_{\mathbf{d}}[y(\mathbf{X})]}{\mathbb{E}_{\mathbf{d}_0}[y(\mathbf{X})]} + w_2 \frac{\sqrt{\text{Var}_{\mathbf{d}}[y(\mathbf{X})]}}{\sqrt{\text{Var}_{\mathbf{d}_0}[y(\mathbf{X})]}}, \\ & -5.12 \leq d_i \leq 5.12, \quad i = 1, \dots, M, \end{aligned}$$

where $y(\mathbf{X})$ is the Rastrigin function:

$$y(\mathbf{X}) = 10N + \sum_{i=1}^N [X_i^2 - 10 \cos(2\pi X_i)].$$

We set equal weight coefficients $w_1 = w_2 = 0.5$. The terms $\mathbb{E}_{\mathbf{d}_0}[y(\mathbf{X})]$ and $\sqrt{\text{Var}_{\mathbf{d}_0}[y(\mathbf{X})]}$ denote the mean and standard deviation at the initial design \mathbf{d}_0 , respectively, serving as normalization factors.

The Rastrigin function is a widely used multi-modal benchmark with numerous local minima, posing a significant challenge for locating the global optimum. Fig. 7 presents that this function has a unique global minimum at the origin $(0, 0)^\top$.

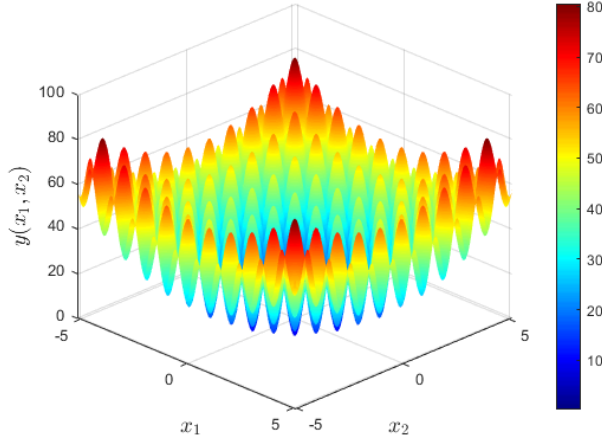


Figure 7: Visualization of the two-dimensional Rastrigin function. The highly multimodal landscape with numerous local minima highlights the difficulty of locating the global optimum at the origin.

4.1.2. Method

We perform RDO for both the two-dimensional (2D) problem (Case 1) and the ten-dimensional (10D) problem (Case 2) problems using three methods: BNN-PDD MPSS, GP-PDD MPSS, and direct MCS. For fair comparison, we train both the BNN and GP surrogates using 500 training samples identically generated through LHS in each subregion.

4.1.3. Results for Case 1 ($N = M = 2$)

Figure 8 shows the convergence history of the objective function for both Cases 1 and 2. The horizontal axis represents the subregion iteration index, and the vertical axis indicates the corresponding objective function value. Since no initial design point is prescribed, we use $\mathbf{d}^{(0)}$ obtained in Step 1 of Section 3.4 as the initial design; consequently, the initial values for BNN and GP differ. As shown in Fig. 8(a), both BNN-PDD MPSS and GP-PDD MPSS converge stably, with the objective function decreasing monotonically over iterations. In Case 1, both the BNN and GP-based approaches reaches the vicinity of the global optimum.

Figure 9(a) and (b) present the PDFs for the initial and optimal designs in Case 1. Both methods produce sharp peaks centered at zero in the optimal design distributions, in contrast to the initial design distributions. This result is attributed to the relatively high data density in the low-dimensional space, which provides sufficient prediction accuracy for both surrogate models. Table 1 confirms that both methods achieve the global optimum, reducing the mean to approximately 0.0043.

4.1.4. Results for Case 2 ($N = M = 10$)

Unlike Case 1, the high-dimensional problem in Case 2 reveals clear performance differences among the three methods. Although Fig 8(b) shows that both BNN-PDD MPSS and GP-PDD MPSS reduce the objective function value over iterations, Fig 9 shows a distinct difference. As shown in Fig 9(d), the GP-based method reduces the standard deviation by 96.95%, yet the mean remained at 4.0044, producing a distribution biased away from zero. This indicates that the GP kernel performance degrades with increasing dimensionality, reducing prediction accuracy and causing the optimizer to become trapped in a local optimum. In contrast, Fig 9(c) demonstrates the robustness of the BNN-based method, where the PDF remains centered at zero even in the high-dimensional setting. This confirms that BNN effectively captures complex variable interactions, enabling accurate exploration of the global optimum in high-dimensional spaces. MCS, meanwhile, fails to identify a meaningful optimal solution within the allowed computational budget. The curse of dimensionality causes the search

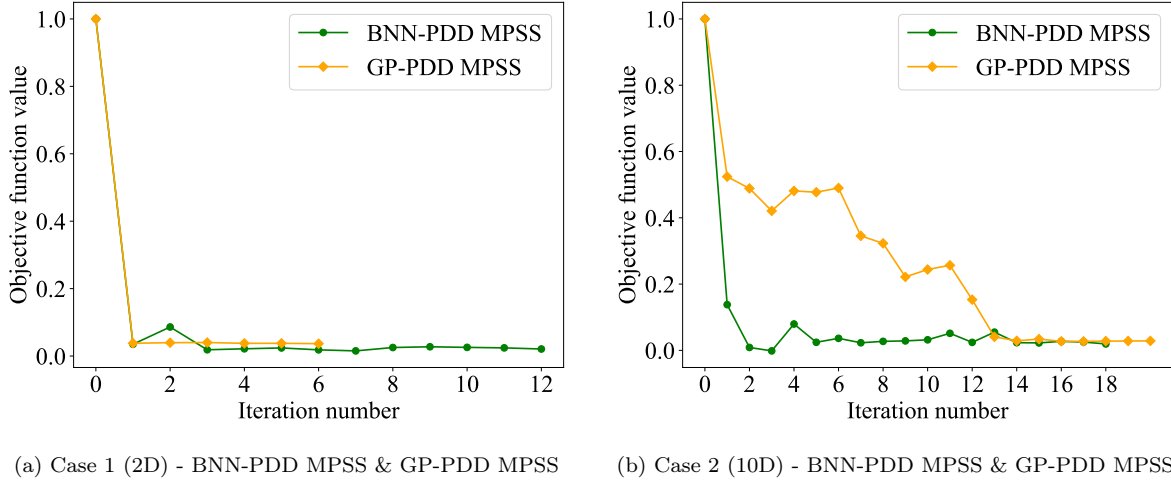


Figure 8: Optimization convergence history of the objective function: (a) Case 1 using BNN-PDD MPSS and GP-PDD MPSS, (b) Case 2 using BNN-PDD MPSS and GP-PDD MPSS.

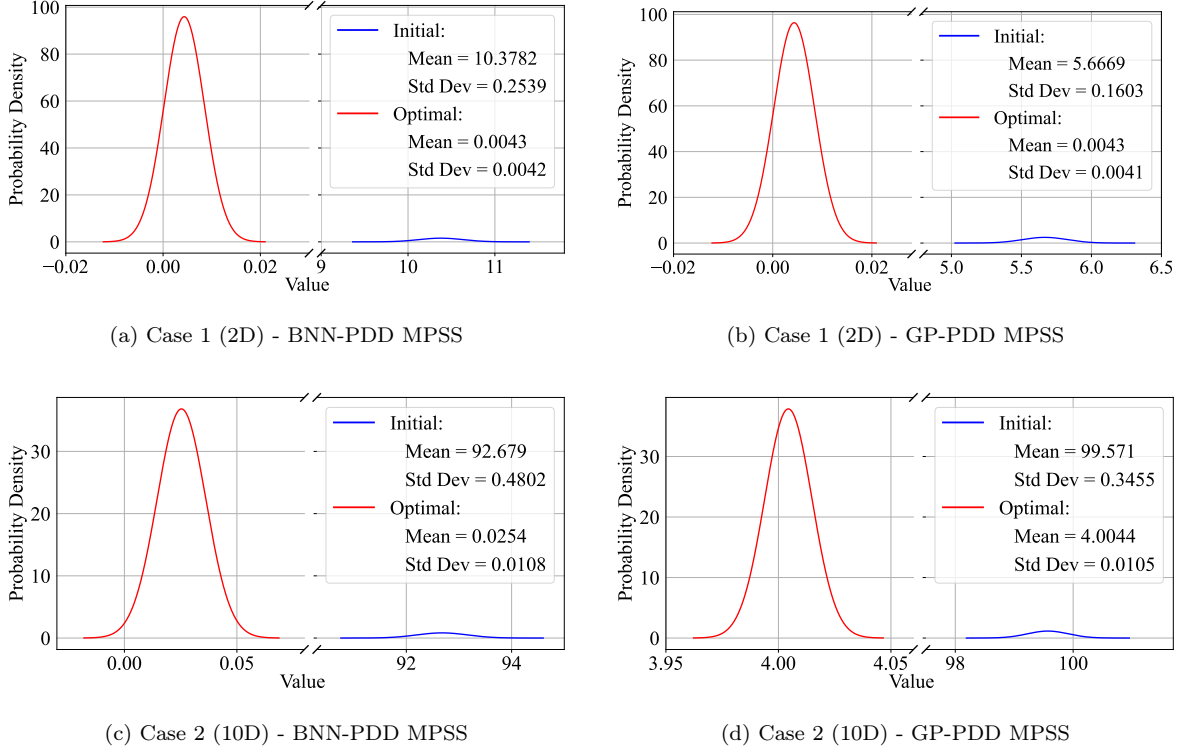


Figure 9: Comparison of PDF results for initial (blue) and optimal (red) designs between the proposed BNN-PDD MPSS and GP-PDD MPSS: (a) BNN-PDD MPSS results for Case 1 (2D), (b) GP-PDD MPSS results for Case 1 (2D), (c) BNN-PDD MPSS results for Case 2 (10D), (d) GP-PDD MPSS results for Case 2 (10D).

space to expand exponentially, making simple random search unable to locate the global optimum of the highly multimodal Rastrigin function.

Table 1 summarizes the quantitative comparison. In Case 2, the GP-based method yields a final mean of 4.0044, while MCS produces a mean of 16.1134, both failing to reach the global optimum. In contrast, BNN-PDD MPSS reduces the mean to 0.0254 and the standard deviation to 1.0831×10^{-2} ,

Table 1: Optimization results for Example 1

	Method	Statistics	Initial ($\mathbf{d}_0^{(0)}$)	Optimal (\mathbf{d}^*)	Reduction (%)	No. of y evaluations
Case 1 (2D)	BNN-PDD MPSS	Mean	10.3782	0.0043	99.96	8300
		Std Dev	2.5393×10^{-1}	4.1584×10^{-3}	98.36	
	GP-PDD MPSS	Mean	5.6669	0.0043	99.92	4800
		Std Dev	1.6034×10^{-1}	4.1399×10^{-3}	97.42	
Case 2 (10D)	direct MCS	Mean	-	0.03884	-	75000
		Std Dev	-	5.1674×10^{-2}	-	
	BNN-PDD MPSS	Mean	92.6790	0.0254	99.97	16400
		Std Dev	4.8018×10^{-1}	1.0831×10^{-2}	97.78	
	GP-PDD MPSS	Mean	99.571	4.0044	95.98	20300
		Std Dev	3.4549×10^{-1}	1.0536×10^{-2}	96.95	
	direct MCS	Mean	-	16.1134	-	1.977×10^6
		Std Dev	-	2.5816×10^{-1}	-	

confirming its ability to accurately and robustly locate the global optimum even in high-dimensional problems.

4.2. Example 2: Shape design of the electric motor

The second example addresses the shape optimization of an external rotor permanent magnet synchronous motor (ERPMMSM). In this configuration, the rotor is located outside the stator, which secures a larger air gap radius compared to conventional inner rotor motors and thus delivers higher torque density within the same volume. This motor type is widely adopted in applications demanding high torque with compact form factors and constant-speed operation, such as drones, cooling fans, and robotics.

Cogging torque arises from the magnetic attraction between the permanent magnets and the stator core even in the absence of excitation, and constitutes the primary source of motor vibration and noise. Minimizing cogging torque through design optimization is therefore critical. However, the complex nonlinear relationships between design variables and motor performance require FEA, which imposes high computational cost and makes RDO particularly challenging. Building on the validation results from Section 4.1, this example evaluates the efficiency and robustness of the proposed BNN-PDD MPSS method as a practical motor design optimization strategy.

4.2.1. Problem definition

The ERPMMSM model used in this example is a surface-mounted permanent magnet synchronous motor with 8 poles and 12 slots. The poles refer to the number of permanent magnets attached to the rotor that generate magnetic flux, while the slots denote the number of grooves accommodating the stator windings. Figure 10 illustrates the two-dimensional electromagnetic field analysis model. We verified the FEA model through a comparative study with [28]: a cogging torque comparison at a magnet pole arc corresponding to a full pole pitch yielded a relative error of approximately 0.69%.

The motor operates at the rated speed of 750 rpm with an axial length of 50 mm. We adopt neodymium magnets with a relative permeability of 1.05 and a remanence of 0.85T and apply AISI 1010 steel for the iron core.

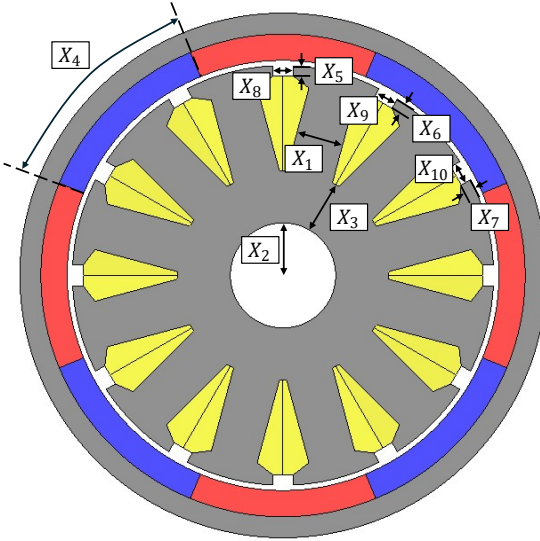


Figure 10: 2D electromagnetic field analysis model of 8-pole 12-slot ERPMSM with random variables. Red and blue represent N and S poles of permanent magnets, yellow indicates the coil winding area, and gray represents iron core.

We leverage the geometric symmetry of the motor to efficiently model manufacturing tolerances. In the 8-pole, 12-slot topology, the greatest common divisor of the pole and slot numbers is four, indicating that both the electromagnetic flux distribution and the geometry repeat four times per mechanical revolution. We therefore construct a one-quarter model, which represents the minimal periodic unit. We define random variables exclusively for the geometric dimensions of the first quarter sector. The remaining three sectors periodically replicate these values.

To incorporate manufacturing uncertainties, we model the geometric dimensions as random variables. We define a total of 10 random variables $\mathbf{X} = (X_1, \dots, X_{10})^\top$, each following a truncated Gaussian distribution. For the stator tooth dimensions d_5 and d_6 , independent manufacturing tolerances can occur at each of the three slots within the one-quarter model. We therefore model these dimensions using three independent random variables each $X_5 \sim X_7$ and $X_8 \sim X_{10}$, respectively. Table 2 summarizes the random variables, manufacturing tolerances, and design ranges. We define the design variables as the mean values of the corresponding random variable. The six design variables are $d_k = \mathbb{E}[\mathbf{X}_k]$ for $k = 1, 2, 3, 4$, $d_5 = \mathbb{E}[\mathbf{X}_5] = \mathbb{E}[\mathbf{X}_6] = \mathbb{E}[\mathbf{X}_7]$, and $d_6 = \mathbb{E}[\mathbf{X}_8] = \mathbb{E}[\mathbf{X}_9] = \mathbb{E}[\mathbf{X}_{10}]$.

We evaluate cogging torque through electromagnetic field analysis under a no-load condition as cogging torque arises without electrical excitation. We formulate the RDO problem to simultaneously minimize the mean and standard deviation of the cogging torque. We impose a constraint to ensure that the mean of cogging torque does not exceed the allowable limit $T_{cogging} = 0.39$ Nm. This RDO is defined as

$$\begin{aligned}
 \min_{\mathbf{d} \in \mathcal{D}} \quad & c_0 = w_1 \frac{\mathbb{E}_{\mathbf{d}}[y(\mathbf{X})]}{\mathbb{E}_{\mathbf{d}_0}[y(\mathbf{X})]} + w_2 \frac{\sqrt{\text{Var}_{\mathbf{d}}[y(\mathbf{X})]}}{\sqrt{\text{Var}_{\mathbf{d}_0}[y(\mathbf{X})]}}, \\
 \text{subject to} \quad & c_1 = \frac{\mathbb{E}_{\mathbf{d}}[y(\mathbf{X})] - T_{cogging}}{\mathbb{E}_{\mathbf{d}_0}[y(\mathbf{X})]} \leq 0, \\
 & 2.5 \text{ mm} \leq d_1 \leq 5.0 \text{ mm}, \\
 & 5.0 \text{ mm} \leq d_2 \leq 7.5 \text{ mm}, \\
 & 3.0 \text{ mm} \leq d_3 \leq 5.0 \text{ mm}, \\
 & 31.0^\circ \leq d_4 \leq 45.0^\circ, \\
 & 0.3 \text{ mm} \leq d_5 \leq 1.0 \text{ mm}, \\
 & 0.5 \text{ mm} \leq d_6 \leq 3.0 \text{ mm},
 \end{aligned}$$

Table 2: Statistical properties of random variables of ERPMSM (Example 2)

Random variables	Design variables (Mean)	Tolerance	Min.	Max.	Probability distribution
Tooth body thickness (X_1), mm	d_1	0.04	2.5	5.0	Truncated Gaussian
Stator inner radius (X_2), mm	d_2	0.04	5.0	7.5	Truncated Gaussian
Stator back yoke thickness (X_3), mm	d_3	0.04	3.0	5.0	Truncated Gaussian
PM pole arc (X_4), $^\circ$	d_4	0.04	31.0	45.0	Truncated Gaussian
Tooth tip thickness (X_5, X_6, X_7), mm	d_5	0.04	0.3	1.0	Truncated Gaussian
Slot opening width (X_8, X_9, X_{10}), mm	d_6	0.04	0.5	3.0	Truncated Gaussian

where $\mathbb{E}_{\mathbf{d}_0}[y(\mathbf{X})]$ and $\text{Var}_{\mathbf{d}_0}[y(\mathbf{X})]$ denote the mean and variance of cogging torque at the initial design \mathbf{d}_0 . The initial design vector is $\mathbf{d}_0 = (4.5 \text{ mm}, 5.0 \text{ mm}, 5.0 \text{ mm}, 45.0^\circ, 1.0 \text{ mm}, 2.0 \text{ mm})^\top$, and the weights are set to $w_1 = w_2 = 0.5$.

4.2.2. Method

We apply the proposed BNN-PDD MPSS to construct local surrogate models in each subregion. We generate 500 training samples within the six-dimensional design space for each subregion using LHS.

4.2.3. Results

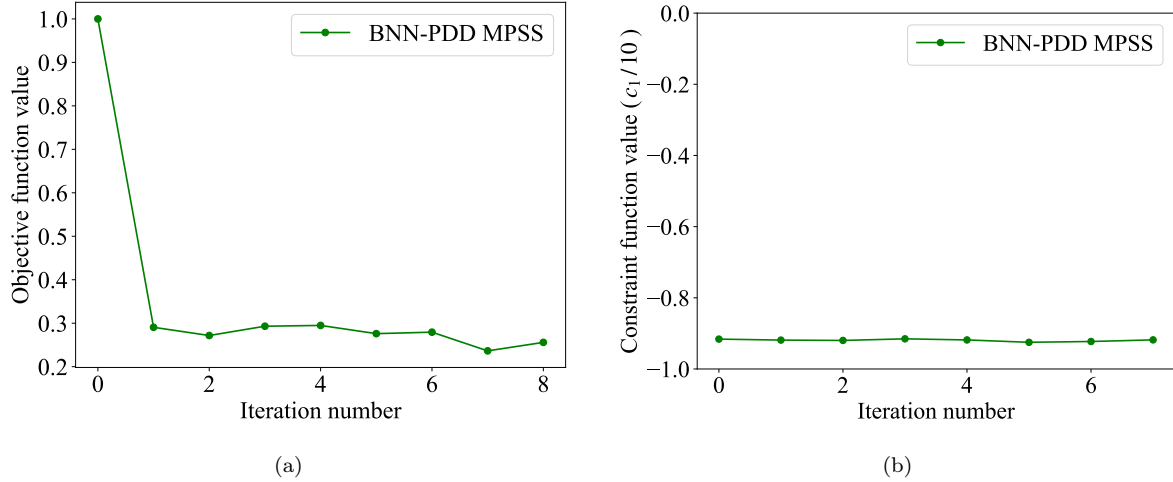


Figure 11: RDO iteration history for Example 2: (a) objective function, and (b) constraint function

Figure 11(a) and (b) show the iteration histories of the objective and constraint functions across subregion iterations. The objective function decreases monotonically, indicating stable convergence.

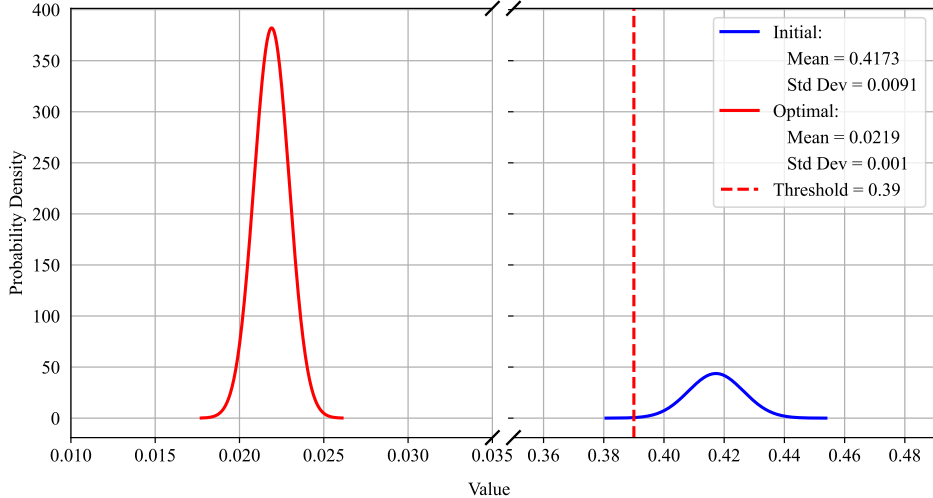


Figure 12: Comparison of PDF results for initial (blue) and optimal (red) designs for Example 2

Figure 12 compares the PDFs of the cogging torque for the initial and optimal designs. The initial design (blue) exhibits a broad distribution centered around 0.42 Nm, lying entirely above the allowable threshold $T_{\text{cog}} = 0.39$ Nm (red dashed line) and thus violating the constraint. In contrast, the optimal design (red) produces a sharp, narrow peak concentrated near 0.022 Nm—well below the threshold—confirming that the proposed method simultaneously reduces the mean cogging torque and suppresses its variability while satisfying the constraint. Table 3 summarizes the quantitative

Table 3: Optimization results for Example 2

Statistics	Initial (\mathbf{d}_0)	Optimal (\mathbf{d}^*)	Reduction (%)	No. of FEA
Mean [Nm]	0.4173	0.02191	94.75	6644
Std Dev [Nm]	9.1274×10^{-3}	1.0444×10^{-3}	88.56	

results. The proposed BNN-PDD MPSS method reduces the mean cogging torque from 0.4173 Nm to 0.02191 Nm (94.75% reduction) and the standard deviation from 9.1274×10^{-3} Nm to 1.0444×10^{-3} Nm (88.56% reduction), achieving both performance improvement and robustness enhancement with only 6644 FEA evaluations. This result confirms that the proposed method effectively handles complex electromagnetic field problems, delivering a robust optimal design even in a high-dimensional, strongly nonlinear setting. Figure 13 compares the 2D topologies of the initial and optimal designs.

5. Conclusion

This study proposed a novel RDO method that integrates BNN with PDD. The combined method leverages BNN as a surrogate to replace expensive model evaluations required for PDD coefficient calculation, enabling rapid estimation of statistical moments at significantly reduced computational cost. The proposed method maximizes sampling efficiency through an active learning strategy driven by BNN predictive uncertainty. Adopting a MPSS strategy, the method partitions the design space into subregions and constructs local surrogate models, while employing a global search within each subregion to handle severe nonlinearity. A dynamic resizing strategy further adjusts subregion boundaries during optimization to avoid entrapment in local optima and enhance search robustness. PDD is then applied to the resulting surrogate, exploiting the structural decomposition of component functions for efficient and accurate probabilistic analysis.

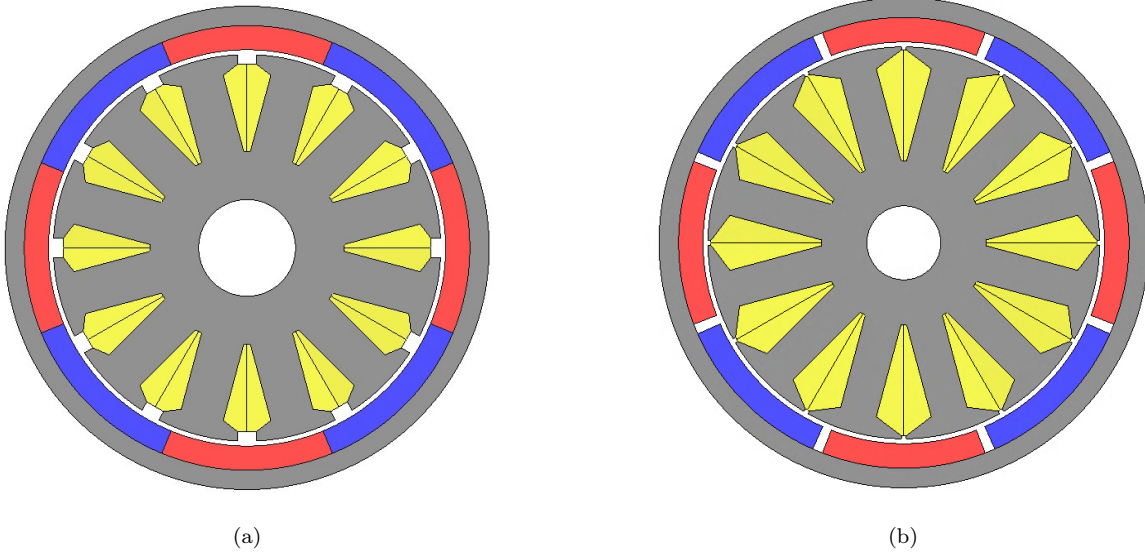


Figure 13: Comparison of the 2D topology between (a) initial design and (b) optimal design of the ERPMSM.

Numerical results confirmed that the proposed method converges stably to optimal solutions with significantly fewer function evaluations compared to conventional approaches. In the high-dimensional Rastrigin problem ($N = 10$), BNN-PDD MPSS achieved a 99.97% mean reduction, while GP-PDD MPSS and MCS failed to locate the global optimum. In the ERPMSM design problem, the method reduced the mean cogging torque by 94.75% and the standard deviation by 88.56% with only 6644 FEA evaluations, demonstrating its practicality for high-dimensional, strongly nonlinear engineering problems.

The proposed method provides an effective solution for robust design of complex engineering systems requiring high-fidelity analysis. However, BNN has inherent limitations: the training process is more complex than that of conventional neural networks, and determining optimal hyperparameters and prior distributions involves relatively high computational cost and sensitivity. The Bayesian optimization-based tuning used in this study required iterative model retraining to identify optimal hyperparameters, resulting in substantial computational overhead. Future work will focus on introducing algorithms that simultaneously optimize weights and hyperparameters during the training process, eliminating the need for iterative retraining and further improving the overall efficiency of the method.

Acknowledgment

This work was supported by Institute of Information & Communications Technology Planning & Evaluation (IITP) grant funded by the Korea government (MSIP) (No. RS-2025-02304285, Development of Digital Triplet Based Predictive Maintenance Solution for Future Power Facility Innovation).

Conflict of Interest

On behalf of all authors, the corresponding author states that there is no conflict of interest.

Replication of Results

All BNN architecture details, PDD truncation parameters, MPSS tolerances, and active learning criteria are fully specified in Section ???. Due to the proprietary nature of the FEA model used in the

motor design example, the simulation files cannot be made publicly available. The source code for the proposed BNN-PDD MPSS method is available from the corresponding author upon request.

References

- [1] Genichi Taguchi. *Taguchi on Robust Technology Development: Bringing Quality Engineering Upstream*. ASME Press, January 1993.
- [2] Zissimos P Mourelatos and Jinghong Liang. A methodology for trading-off performance and robustness under uncertainty. *J. Mech. Des.*, 128(4):856–863, 2006.
- [3] Kais Zaman, Mark McDonald, Sankaran Mahadevan, and Lawrence Green. Robustness-based design optimization under data uncertainty. *Structural and Multidisciplinary Optimization*, 44(2):183–197, 2011.
- [4] Gyung-Jin Park, Tae-Hee Lee, Kwon Hee Lee, and Kwang-Hyeon Hwang. Robust design: an overview. *AIAA journal*, 44(1):181–191, 2006.
- [5] Wen Yao, Xiaoqian Chen, Wencai Luo, Michel Van Tooren, and Jian Guo. Review of uncertainty-based multidisciplinary design optimization methods for aerospace vehicles. *Progress in Aerospace Sciences*, 47(6):450–479, 2011.
- [6] Nuri Kim, Yoojeong Noh, Gyungmin Choi, Dong Jun Oh, Young-Jin Kang, Noma Park, and Soonyong Choi. Deep reinforcement Nelder-Mead optimization for Hvac digital twin model performance. *Available at SSRN 4883196*.
- [7] Dongjin Lee and Sharif Rahman. Practical uncertainty quantification analysis involving statistically dependent random variables. *Applied Mathematical Modelling*, 84:324–356, 2020.
- [8] Mingyu Lee, Yoojeong Noh, and Ikjin Lee. A novel sampling method for adaptive gradient-enhanced Kriging. *Computer Methods in Applied Mechanics and Engineering*, 418:116456, 2024.
- [9] Hojoon Cho, Sangmin Seo, Chinseok Heo, Junjae Kwak, Yongbae Kim, Jinsoo Park, Sangjun Lee, and Seongsik Lim. Performance estimation of freeze protection system for outdoor fire piping by using AI algorithm. *Journal of Mechanical Science and Technology*, 37(10):5093–5101, 2023.
- [10] Yulin Guo and Boris Kramer. Risk-based design optimization for powder bed fusion metal additive manufacturing. *Structural and Multidisciplinary Optimization*, 68(9):179, 2025.
- [11] Dongjin Lee and Boris Kramer. Multifidelity conditional value-at-risk estimation by dimensionally decomposed generalized polynomial chaos-Kriging. *Reliability Engineering & System Safety*, 235:109208, 2023.
- [12] Yeonsu Kim, Junhan Lee, Bingran Wang, John T Hwang, and Dongjin Lee. Interpolation-based optimal knot selection in spline dimensional decomposition for uncertainty quantification in dynamical systems. *Applied Mathematical Modelling*, page 116613, 2025.
- [13] Jaeyub Hyun, Anirban Chaudhuri, Karen E Willcox, and H Alicia Kim. Robust topology optimization of continuum structures under material uncertainties using multifidelity Monte Carlo. *Computer Methods in Applied Mechanics and Engineering*, 451:118714, 2026.
- [14] Lebede Ngartera, Mahamat Ali Issaka, and Saralees Nadarajah. Application of bayesian neural networks in healthcare: three case studies. *Machine Learning and Knowledge Extraction*, 6(4):2639–2658, 2024.
- [15] Niko Hauzenberger, Florian Huber, Karin Klieber, and Massimiliano Marcellino. Bayesian neural networks for macroeconomic analysis. *Journal of Econometrics*, 249:105843, 2025.

- [16] Minsuk Song, Ryun-Han Koo, Jangsaeng Kim, Chang-Hyeon Han, Jiyong Yim, Jonghyun Ko, Sijung Yoo, Duk-hyun Choe, Sangwook Kim, Wonjun Shin, et al. Ferroelectric nand for efficient hardware bayesian neural networks. *Nature Communications*, 16(1):6879, 2025.
- [17] Sharif Rahman. A polynomial dimensional decomposition for stochastic computing. *International Journal for Numerical Methods in Engineering*, 76(13):2091–2116, 2008.
- [18] Yulin Guo, Dongjin Lee, and Boris Kramer. Robust design optimization with limited data for char combustion. *Structural and Multidisciplinary Optimization*, 68(3):1–18, 2025.
- [19] Dongjin Lee and Sharif Rahman. Robust design optimization under dependent random variables by a generalized polynomial chaos expansion. *Structural and Multidisciplinary Optimization*, 63(5):2425–2457, 2021.
- [20] Sharif Rahman. Statistical moments of polynomial dimensional decomposition. *Journal of engineering mechanics*, 136(7):923–927, 2010.
- [21] Ethan Goan and Clinton Fookes. Bayesian neural networks: An introduction and survey. In *Case Studies in Applied Bayesian Data Science: CIRM Jean-Morlet Chair, Fall 2018*, pages 45–87. Springer, 2020.
- [22] David JC MacKay. A practical bayesian framework for backpropagation networks. *Neural computation*, 4(3):448–472, 1992.
- [23] Michael I Jordan, Zoubin Ghahramani, Tommi S Jaakkola, and Lawrence K Saul. An introduction to variational methods for graphical models. *Machine learning*, 37(2):183–233, 1999.
- [24] Alex Graves. Practical variational inference for neural networks. *Advances in neural information processing systems*, 24, 2011.
- [25] Jon C Helton and Freddie Joe Davis. Latin hypercube sampling and the propagation of uncertainty in analyses of complex systems. *Reliability Engineering & System Safety*, 81(1):23–69, 2003.
- [26] Hans Janssen. Monte-carlo based uncertainty analysis: Sampling efficiency and sampling convergence. *Reliability Engineering & System Safety*, 109:123–132, 2013.
- [27] Vassili V Toropov, AA Filatov, and AA Polynkin. Multiparameter structural optimization using fem and multipoint explicit approximations. *Structural optimization*, 6(1):7–14, 1993.
- [28] PP Ling, Dahaman Ishak, and TL Tiang. Influence of magnet pole arc variation on the performance of external rotor permanent magnet synchronous machine based on finite element analysis. In *2016 IEEE International Conference on Power and Energy (PECon)*, pages 552–557. IEEE, 2016.